

PAPER

^{90}Y TOF-PET based EUD reunifies patient survival prediction in resin and glass microspheres radioembolization of HCC tumours

To cite this article: P d'Abadie *et al* 2018 *Phys. Med. Biol.* **63** 245010

View the [article online](#) for updates and enhancements.

You may also like

- [Performance of a dual-layer scanner for hybrid SPECT/CBCT](#)
Martijn M A Dietze, Britt Kunnen, Sandra van der Velden *et al.*
- [Systematic investigation on the validity of partition model dosimetry for \$^{90}\text{Y}\$ radioembolization using Monte Carlo simulation](#)
Nurul Ab Aziz Hashikin, Chai-Hong Yeong, Susanna Guatelli *et al.*
- [Impact of image reconstruction method on dose distributions derived from \$^{90}\text{Y}\$ PET images: phantom and liver radioembolization patient studies](#)
Xinchi Hou, Hillgan Ma, Pedro L Esquinas *et al.*

JOIN US | ESTRO 2024
**In-Booth Talks, Demos,
& Lunch Symposium**

[Browse talk schedule >](#)

SUN NUCLEAR
A MEDTRONIC MEDICAL COMPANY



PAPER

^{90}Y TOF-PET based EUD reunifies patient survival prediction in resin and glass microspheres radioembolization of HCC tumours

P d'Abadie, M Hesse, F Jamar, R Lhommel and S Walrand

Nuclear Medicine, Saint-Luc Hospital, Brussels, Belgium

E-mail: stephan.walrand@uclouvain.be and philippe.dabadie@uclouvain.be

Keywords: radioembolization, TOF-PET/CT, EUD, dosimetry, survival curve

RECEIVED
10 August 2018REVISED
29 October 2018ACCEPTED FOR PUBLICATION
19 November 2018PUBLISHED
12 December 2018

Abstract

Clinical studies reported a twofold ratio between the efficacies per Gy of resin versus glass spheres. Our aim is to investigate whether this difference could result from the different degrees of heterogeneity in sphere distribution between the two medical devices. The ^{90}Y TOF-PET based equivalent uniform doses (EUD) was used for this purpose.

58 consecutive HCC radioembolizations were retrospectively analyzed. Absorbed doses D and Jones–Hoban EUD in lesions were computed. Radioembolization efficacy was assessed using Kaplan–Meier survival curves.

In order to match together the glass and resin spheres survival curves using a 40 Gy-threshold, an efficacy factor of 0.73 and 0.36 has to be applied on their absorbed dose, respectively. Using EUD, a nice matching between glass and resin survival curves was obtained with a better separation of the responding and not responding survival curves.

The results clearly support the fact that the activity heterogeneity observed in ^{90}Y TOF-PET post radioembolization does not only result from statistical noise, but also reflects the actual heterogeneity of the spheres distribution. Use of EUD reunifies the efficacy of the two medical devices.

Introduction

Three different medical devices are available in liver radioembolization (Pasciak *et al* 2016): ^{90}Y loaded glass or resin spheres, and, more recently introduced, ^{166}Ho loaded poly L-lactic acid spheres. Glass and resin spheres mainly differ by their specific ^{90}Y activity: about 2500 Bq per glass sphere and about 50 Bq per resin sphere.

Review of clinical studies (Spreafico *et al* 2014) reported a twofold ratio between the toxicities per Gy of resin and of glass spheres, i.e. a whole liver tolerable dose of 70Gy for glass spheres (Chiesa *et al* 2012) and of 40 Gy for resin spheres (Cremonesi *et al* 2008, Sangro *et al* 2008, Strigari *et al* 2010, Lau *et al* 2012). Monte Carlo (MC) simulations of spheres transport in hepatic arterial tree (Walrand *et al* 2014a, 2014b, Crookston *et al* 2018) evidenced that glass spheres give a more heterogeneous dose distribution that quantitatively explains the difference in liver toxicity (Walrand *et al* 2014a). The sphere distribution measured in liver biopsies post radioembolization (Högberg *et al* 2014) was in agreement with the MC simulations (Pasciak *et al* 2016).

Similar ratio between efficacy per Gy has also been reported (Chiesa *et al* 2011) when comparing the results of glass and of resin sphere radioembolization studies in HCC (Strigari *et al* 2010, Mazzaferro *et al* 2013). The aim of this study is to investigate whether this difference is also linked to the sphere distribution heterogeneity in the tumours. This distribution cannot be modelled in a meaningful way regarding the anarchic tumour vasculature. Thus, patient overall survival curves were predicted by the uniform equivalent dose (EUD) computed from the tumour activity distribution assessed by ^{90}Y TOF-PET imaging.

Material and methods

Radioembolizations

A total of 58 consecutive liver radioembolizations (see table 1) in 45 patients with HCC imaged by ^{90}Y TOF-PET were retrospectively analyzed under the approval of the local ethic committee. Patient CHILD scores were A5 ($n = 30$), A6 ($n = 8$), B7 ($n = 2$), B8 ($n = 4$) and B9 ($n = 1$). The radioembolizations were performed according to the standard liver radioembolization guidelines (Kennedy *et al* 2007). Glass and resin spheres were used in 33 and 25 radioembolizations with a mean activity of 2.6 and 1.5 GBq, respectively. No decaying was applied on the sphere vials before radioembolization, i.e. specific activity at the treatment day of resin and glass sphere was about 50 and 2500 Bq, respectively.

A 45 min ^{90}Y TOF-PET scan (Gemini TF, Philips Medical Systems, Cleveland, OH, USA) was performed within 4 h ($n = 55$) or within 16 h ($n = 3$) following the radioembolization.

Dose assessment

Voxel absorbed dose distribution was assessed using a validated scheme (Lhommel *et al* 2010). In summary: ^{90}Y activity distribution was reconstructed using the vendor 3D line of response (LOR)–TOF blob-based reconstruction algorithm with 2 iterations and 33 subsets and a $4 \times 4 \text{ mm}^3$ voxel size. Afterwards, an expectation maximization (EM) based spatial resolution recovery was applied. This spatial resolution correction post reconstruction was shown Lhommel *et al* (2010) and van Elmbt *et al* (2011) to provide similar recovery coefficients than that observed from other PET systems including a PSF modelling in the reconstruction (Willowson *et al* 2015). Last, the activity distribution was convolved with the ^{90}Y dose kernel distribution in water taking into account the continuous beta energy spectrum (Cross *et al* 1992).

Volume of interest (VOI) was drawn on up to the nine biggest lesions, if any, using the MRI ($n = 50$) or injected CT scan ($n = 8$) and further fused on the ^{90}Y TOF-PET image. Two dosimetry quantities in the tumour VOIs were evaluated:

The effective absorbed dose D_{eff} obtained by multiplying the conventional mean absorbed dose D with an efficacy factor depending on the medical device, i.e.:

$$D_{\text{eff}} = a_{\text{dev}} D. \quad (1)$$

The Jones and Hoban EUD (Jones and Hoban 2000), which is the uniform dose that would give the same survival fraction than that resulting from the actual dose distribution, i.e.:

$$\text{EUD} = -\frac{1}{\alpha} \ln \left(\frac{\sum_i e^{-\alpha D_i}}{N} \right) \quad (2)$$

where D_i is the absorbed dose in the voxel i inside the tumour VOI, α is the HCC cells radiosensitivity and N the number of voxels contained in the tumour VOI.

Efficacy assessment

Efficacy of each medical device was assessed by analyzing the overall patient survival. In this analyze a total of 26 radioembolizations were censored due to an additional treatment performed in the patient (see table 1), i.e. were withdrawn at that time from the curve and from the overall number of patients. These additional treatments were: additional radioembolization performed in order to target a novel lesion ($n = 13$); additional immunotherapy ($n = 4$); chemotherapy ($n = 3$); additional external beam radiotherapy (EBRT) ($n = 1$); additional chemoembolization ($n = 2$); transplantation ($n = 1$); hepatectomy ($n = 2$). Three radioembolizations were censored, the patient being still alive.

A set of Kaplan–Meyer overall survival curves for the D_{eff} and EUD of the largest lesion being below and above a 40 Gy-threshold were computed from a wide range of discrete radiobiological a_{dev} and α values, respectively. The use of this 40 Gy-threshold derived from EBRT is justified by the fact that the efficacy reduction resulting from the sphere distribution heterogeneity has to be taken into account by equations (1) and (2). The mean tumour diameter was $5.2 \pm 3.2 \text{ cm}$ (see table 1).

Choice of the optimal radiobiological values

The optimal radiobiological values were chosen as the a_{dev} and α values corresponding to the Kaplan–Meyer overall survival curves showing the best agreement between the two medical devices, while preserving a clear separation between the overall survival fraction (OSF) curves corresponding to D_{eff} and EUD lower and higher than a 40 Gy-threshold, respectively, i.e. by maximizing the objective function (O):

$$O = \frac{\sum_t \left| \text{OSF}_{\text{res}}^<(t) - \text{OSF}_{\text{res}}^>(t) \right|^2 + \sum_t \left| \text{OSF}_{\text{glass}}^<(t) - \text{OSF}_{\text{glass}}^>(t) \right|^2}{\sum_t \left| \text{OSF}_{\text{res}}^<(t) - \text{OSF}_{\text{glass}}^<(t) \right|^2 + \sum_t \left| \text{OSF}_{\text{res}}^>(t) - \text{OSF}_{\text{glass}}^>(t) \right|^2}. \quad (3)$$

Where t is the delay post radioembolization.

The justification of computing a set of Kaplan–Meyer overall survival curves for a wide range of discrete radiobiological a_{dev} and α values is linked to the fact that the objective function O is not a continuous function. Conventional fitting algorithms estimating the objective function derivative are not adapted to this feature.

Results

Figure 1 shows the overall survival curves for the two medical devices and using the two dosimetry quantities (1) and (2). The fitted efficacy factors were $a_{\text{res}} = 0.73$ and $a_{\text{glass}} = 0.36$, while the objective function O held on a maximal plateau for α ranging from 0.034 to 0.038 Gy⁻¹. Figure 1(A) shows that it is required to assume different medical device efficacies in order to get similar survival curves. Figure 1(B) shows that the agreement between resin and glass survival curves is further improved when using the EUD (2) with a single fitted parameter rather than using the two empirical efficacy factors (1).

Figure 2 shows the correspondence between the absorbed dose D and the EUD for the tumours having an absorbed dose lower than 120 Gy, i.e. in the region surrounding the 40 Gy-threshold when taking into account the dose efficacy.

Discussion

Taking into account the fitted efficacies (1), the optimal absorbed dose thresholds in order to get a good match between resin and glass sphere overall survival curves, while preserving a clear separation between not responding and responding patients, are 55 and 111 Gy for resin and glass spheres, respectively (figure 1(A)). The efficacy ratio (≈ 2) between resin to glass sphere is in line with that reported in previous studies (Strigari *et al* 2010, Chiesa *et al* 2011, Mazzaferro *et al* 2013).

Assessing the optimal predictive clinical dose threshold between responding and no responding patients was not the purpose of this study. Clinicians are mainly interested in evaluating the impact of a specific medical device radioembolization within a whole treatment frame. Thus, this assessment is usually performed without aiming to get similar survival curves for the two medical devices, and without censoring the radioembolization follow up when the patient get an additional therapy. However, despite these two additional constraints, overall survival duration of responding patients in this study are about twofold that of not responding.

Similar overall survival curves, jointly with a better agreement between the two medical devices, are directly obtained using the EUD for a HCC cells radiosensitivity ranging from 0.034 to 0.038 Gy⁻¹ (figure 1(B)). The fact that a maximal plateau was found rather than a maximal peak is explained by the fact that Kaplan–Meier curves and the objective function O remain constant until a small variation of the radiosensitivity α shifts one patient from one curve to another.

The 40 Gy dose threshold is commonly used for many cancer types in EBRT where the dose distribution is homogeneous. A retrospective study in 155 patients treated by local EBRT for HCC also showed that 40 Gy was the minimal threshold in order to observe some patients with a survival longer than three years (Seong *et al* 2003). The successful utilization of this threshold in this study further supports the correct handling by the TOF-PET based EUD of the dose distribution heterogeneities arising in radioembolization. The relation between EUD and absorbed dose D (figure 2) clearly evidenced that glass spheres distribution in tumour is more heterogeneous than that of resin spheres, explaining the twofold efficacy ratio. The linear fit of EUD versus D gave slopes in line with the medical device efficacies.

We also investigated the impact of using the voxel BED instead of the voxel D in equation (2) as originally proposed by Jones and Hoban (2000). In agreement with Chiesa *et al* (2015), using $\alpha/\beta = 10$ Gy and a repair half life of 1.5 h (Strigari *et al* 2010), only a slight difference between EUD and EUDBED was found (table 1). This results from the fact that for a heterogeneous dose distribution, the cell survival fraction is mainly given by the voxels receiving the small doses for which $\text{BED} \approx D$.

The 40 Gy given in EBRT per 2 Gy fractions corresponds to a BED of 48 Gy. However using the EUDBED with this 48 Gy BED threshold, exactly the same optimal Kaplan–Meier curves than those of figure 1(B) were found but for a radiosensitivity ranging from 0.026 to 0.031 Gy. This observation means that due to the step behaviour of the Kaplan–Meier curves resulting in a finite number of different survival curves, the patient serie is too limited in order to probe the quadratic dependence of the radiobiological effects.

The α value measured by Strigari *et al* in human HCC radioembolization is two orders of magnitude lower than those measured in cell assay (Wigg *et al* 2010). Indeed Strigari *et al* neglected the tumour dose heterogeneity and computed the tumour control probability (TCP) by directly multiplying the mean tumour dose by α . Thus, this α value does not only take into account the intrinsic cell radiosensitivity, but also the reduction of the dose efficacy resulting from the heterogeneous distribution. The value found by Chiesa *et al* and the values found in this study range in between the extrinsic and intrinsic values (the adjective ‘apparent’ used in table 2 was intro-

Table 1. Patients and dosimetry data.

Pat.	Treat.	CHILD	OS [m]	Censoring reason	Device	Diam. [cm]	D [Gy]	EUD [Gy]	EUDBED [Gy]	EUD/D
1	1	A5	5.3		Resin	5.1	38	26	28	0.69
2	1	A5	3.3		Resin	13.6	24	16	16	0.66
3	1	A6	>2.5	Additional RE	Glass	5.1	121	36	37	0.30
3	2	A6	5.8		Glass	2.7	58	25	26	0.44
4	1	A5	7.0		Glass	3.8	254	70	72	0.27
5	1	B8	>6	Additional nexavar	Glass	6.8	96	24	24	0.24
6	1	A5	>2.6	Additional Nexavar	Glass	4.0	95	57	61	0.60
7	1	A5	>16	Additional RE	Glass	3.3	87	48	51	0.55
7	2	A5	17.3		Glass	2.9	320	199	246	0.62
8	1	A5	>6	Additional RE	Glass	5.7	414	65	67	0.16
8	2	A6	16.0		Glass	2.3	227	80	83	0.35
9	1	A6	5.6		Glass	12.0	109	39	40	0.36
10	1	A6	12.7		Glass	4.0	94	24	24	0.25
11	1	A6	21.0		Glass	5.5	148	53	55	0.36
12	1	B7	>1.8	Additional nexavar	Glass	10.6	68	23	23	0.33
13	1	A5	>3	Additional RE	Glass	8.3	140	72	76	0.52
13	2	A5	>3		Glass	6.2	169	93	100	0.55
14	1	A5	12.3		Glass	9.8	135	49	49	0.36
15	1	A5	10.3		Resin	9.2	15	10	11	0.71
16	1	B8	>1.8		Glass	3.6	307	136	146	0.44
17	1	B8	18.0		Glass	3.7	251	90	93	0.36
18	1	A6	12.4		Glass	2.0	450	144	155	0.32
19	1	A5	>6	Additional RE	Glass	7.3	253	47	49	0.19
19	2	A5	>6	Additional RE	Resin	1.1	66	61	69	0.92
19	3	A5	3.4		Resin	4.7	69	25	25	0.36
20	1	A5	>12	Additional RE	Glass	4.5	210	103	108	0.49
20	2	A5	9.8		Resin	1.3	397	43	43	0.11
21	1	B7	2.9		Glass	7.7	97	58	62	0.60
22	2	A5	20.0		Resin	3.3	334	96	100	0.29
23	1	A5	>3	Additional RE	Glass	3.3	402	94	98	0.24
23	2	A5	26.0		Resin	3.2	174	96	107	0.55
24	1	A5	3.0		Resin	2.0	56	47	47	0.85
25	1	A6	8.3		Glass	6.6	137	110	110	0.80
26	1	B9	5.2		Resin	2.6	13	14	14	1.05
27	1	A5	>6.7	Additional RE	Resin	7.0	227	93	98	0.41
27	2	A5	>26.3	Additional EBRT	Glass	6.2	785	107	111	0.14
28	1	A5	>21	Additional RE	Resin	3.3	81	49	52	0.61
28	2	A5	>8.2	Still alive	Resin	4.0	204	62	65	0.31
29	1	A5	14.8		Resin	6.7	82	48	48	0.58
30	1	A6	>4	Additional RE	Resin	1.8	50	29	30	0.59
30	2	A6	>3	Additional CE	Glass	1.7	198	50	50	0.25
31	1	A5	16.0		Resin	2.5	314	115	115	0.37
32	1	A5	>3	Additional chemo	Resin	10.6	76	46	49	0.61
33	1	A5	>2	Additional chemo	Resin	2.9	102	106	106	1.04
34	1	B8	3.1		Glass	5.1	451	82	85	0.18
35	1	A5	2.9		Glass	12.0	74	36	38	0.48
36	1	A5	>5	Additional Nexavar	Resin	6.9	26	16	17	0.62
37	1	A5	>16.2	Still alive	Resin	2.8	158	76	81	0.48
38	1	A5	5.8		Resin	8.2	137	51	51	0.37
39	1	A6	>8	Transplantation	Resin	1.4	143	114	134	0.80
40	1	A5	>2	Additional RE	Resin	9.8	57	31	32	0.54
40	2	A5	>9.8	Hepatectomy	Glass	2.0	271	89	93	0.33
41	1	A5	8.7		Glass	8.4	134	66	69	0.49
42	1	A5	>4	Additional RE	Glass	7.3	225	94	100	0.42
42	2	A5	>7.9	Additional CE	Glass	5.0	592	182	195	0.31
43	1	A5	>5	Hepatectomy	Glass	4.3	1426	106	108	0.07
44	1	A5	>5.4	Additional chemo	Resin	2.7	55	48	52	0.87
45	1	A5	>9.8	Still alive	Resin	3.0	143	60	63	0.42

RE: radioembolization, CE: chemo-embolization, chemo: chemotherapy, OS: overall survival duration, censoring time is indicated by the symbol >.

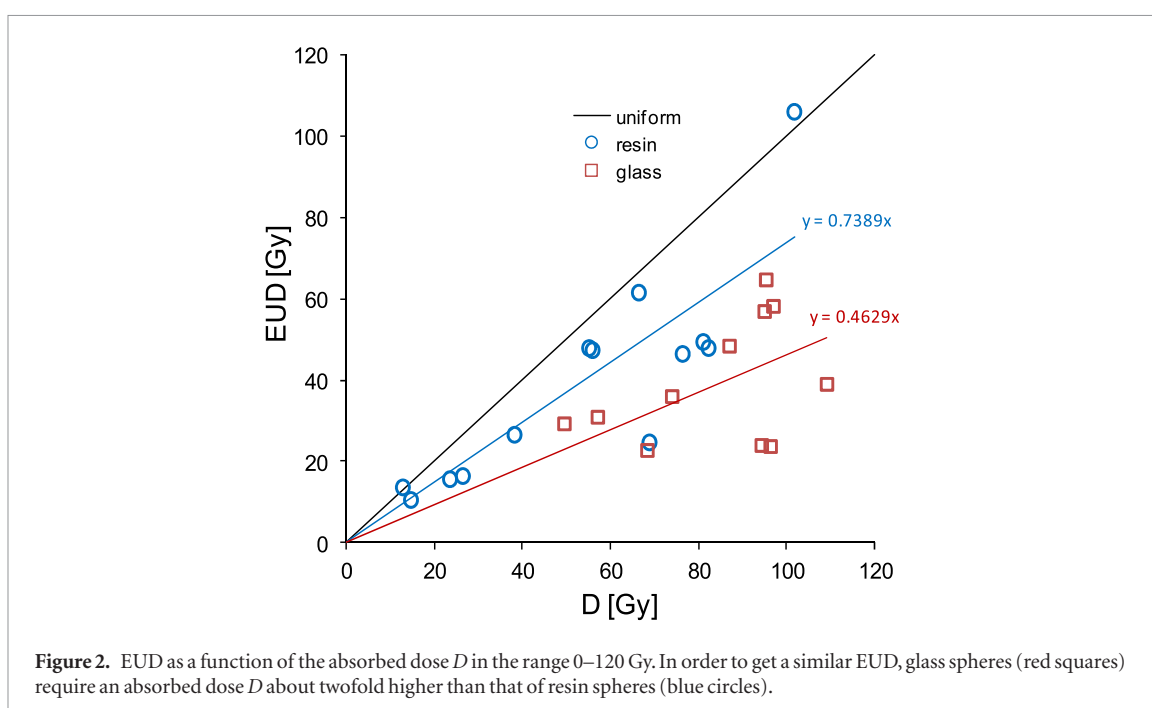
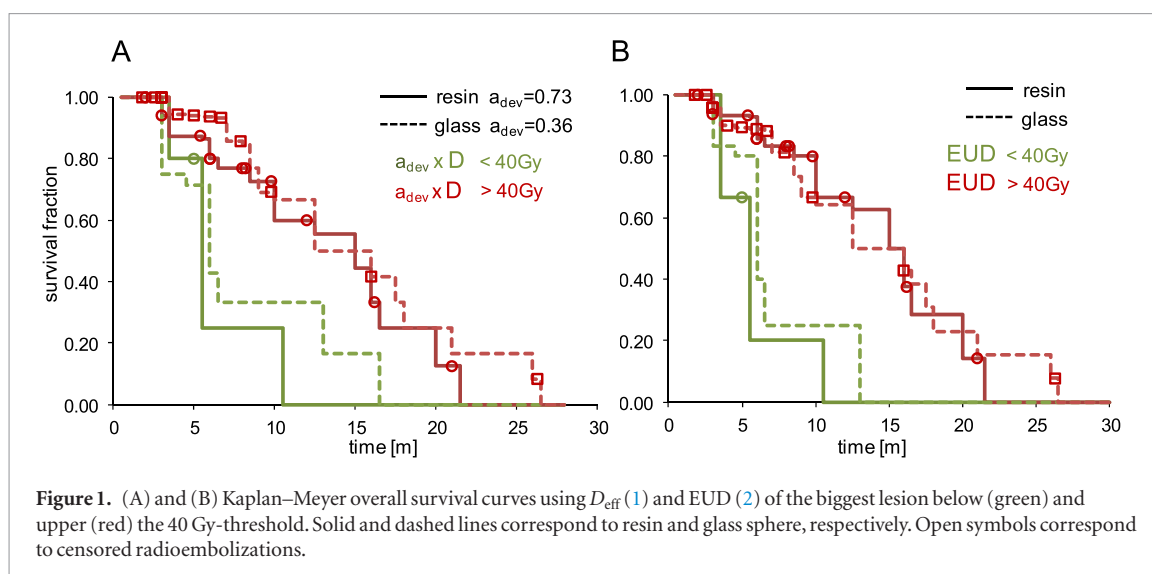


Table 2. Summarizes the different assessments of the radiosensitivity α reported in the literature.

	Derived from	α [Gy^{-1}]	α type	Input distribution:	Spatial resolution
Strigari <i>et al</i> (2010)	Human <i>in vivo</i>	0.001	Extrinsic	Tumour mean dose	Tumour diameter
Chiesa <i>et al</i> (2015)	Human <i>in vivo</i>	0.003	Apparent	$^{99\text{m}}\text{TcMAA}$ -SPECT/CT	≈ 1.5 cm
This study EUDBED	Human <i>in vivo</i>	0.026–0.031	Apparent	^{90}Y TOF-PET/CT	≈ 0.7 cm
This study EUD	Human <i>in vivo</i>	0.034–0.038	Apparent	^{90}Y TOF-PET/CT	≈ 0.7 cm
Wigg <i>et al</i> (2010)	Cell assay	0.1–0.43	Intrinsic	Uniform irradiation	Cell level

duced by Chiesa *et al*). Indeed the SPECT and PET imaging takes into account the intra-tumour dose distribution up to a certain point depending on their effective spatial resolution.

Quite interestingly, these results support that the activity heterogeneities observed in ^{90}Y TOF-PET post radioembolization do not only arise from statistical noise, but mainly represent the actual spheres distribution. This was already evidenced in liver tissue by MC simulations of spheres transport in the hepatic arterial tree (Walrand *et al* 2014a, Crookston *et al* 2018) in which simulated sphere distribution texture matched that observed in ^{90}Y TOF-PET imaging. This was still more expected in tumour tissue that takes up about fourfold more spheres per g than the liver tissue, which results in lower statistical noise.

To our knowledge, it is the first time that the use of EUD was shown to provide a better separation between responding and not responding patients. More valuably, the ^{90}Y TOF-PET based EUD directly allows taking into account the actual sphere distribution and also the actual activity per sphere that can be tuned by decaying the spheres vial before radioembolization. EUD should also directly be usable for the ^{166}Ho loaded spheres.

When an additional radioembolization was performed in a patient in order to target a novel threatening lesion, the follow up of the previous radioembolization was censored. The new radioembolization was then followed with regards to the dosimetry quantities of this novel lesion which, by becoming the major threat to the patient life at that time, has triggered the additional radioembolization. This justifies the use of the biggest lesion alone to build the survival curves, regarding that a smaller lesion will trigger an additional treatment if it progresses. A literature review of 72 studies including a total of 23 968 patients showed that the size of the largest region had a major impact on the patient survival (Tandon and Garcia-Tsao 2009). This impact was also observed in the previously cited local EBRT treatments of HCC (Seong *et al* 2003).

The present study suffers from the limitation that the radioembolization medical device was not randomly chosen, but was chosen in function of the HCC pattern requiring or not a highly selective radioembolization. However, it should be very unlikely that this could have induced a bias leading to the success in using the EUD.

Conclusion

The results clearly support the fact that the heterogeneity observed in ^{90}Y TOF-PET post radioembolization does not only result from low statistics, but also reflects the actual heterogeneity of the spheres distribution. Using realistic HCC radiosensitivity, ^{90}Y TOF-PET based EUD reunifies the efficacy of the two medical devices.

Disclosure

The authors declare to have no conflict of interest to disclose.

There was no financial support.

References

- Chiesa C *et al* 2011 Need, feasibility and convenience of dosimetric treatment planning in liver selective internal radiation therapy with (^{90}Y) microspheres: the experience of the National Tumor Institute of Milan *Eur. J. Nucl. Med. Mol. Imaging* **55** 168–97
- Chiesa C *et al* 2012 A dosimetric treatment planning strategy in radioembolization of hepatocarcinoma with ^{90}Y glass microspheres *Eur. J. Nucl. Med. Mol. Imaging* **56** 503–8
- Chiesa C *et al* 2015 Radioembolization of hepatocarcinoma with ^{90}Y glass microspheres: development of an individualized treatment planning strategy based on dosimetry and radiobiology *Eur. J. Nucl. Med. Mol. Imaging* **42** 1718–38
- Cremonesi M *et al* 2008 Radioembolization with ^{90}Y -microspheres: dosimetric and radiobiological investigation for multi-cycle treatment *Eur. J. Nucl. Med. Mol. Imaging* **35** 2088–96
- Crookston N R, Fung G S and Frey E C 2018 Development of a customizable hepatic arterial tree and particle transport model for use in treatment planning *IEEE Trans. Radiat. Plasma Med. Sci.* **31**
- Cross W G, Freedman N O and Wong P Y 1992 Tables of beta-ray dose distributions in water Report No AECL-10521 Atomic Energy of Canada, Ltd, Ontario, Canada
- Högberg J *et al* 2014 Heterogeneity of microsphere distribution in resected liver and tumour tissue following selective intrahepatic radiotherapy *EJNMMI Res.* **4** 48
- Jones L C and Hoban P W 2000 Treatment plan comparison using equivalent uniform biologically effective dose (EUBED) *Phys. Med. Biol.* **45** 159–70
- Kennedy A *et al* 2007 Recommendations for radioembolization of hepatic malignancies using yttrium-90 microsphere brachytherapy: a consensus panel report from the radioembolization brachytherapy oncology consortium *Int. J. Radiat. Oncol. Biol. Phys.* **68** 13–23
- Lau W Y *et al* 2012 Patient selection and activity planning guide for selective internal radiotherapy with yttrium-90 resin microspheres *Int. J. Radiat. Oncol. Biol. Phys.* **82** 401–7
- Lhommel R *et al* 2010 Feasibility of ^{90}Y TOF PET-based dosimetry in liver metastasis therapy using SIR-Spheres *Eur. J. Nucl. Med. Mol. Imaging* **37** 1654–62
- Mazzaferro V *et al* 2013 Yttrium-90 radioembolization for intermediate-advanced hepatocarcinoma: a phase II study *Hepatology* **57** 1826–37
- Pasciak A S, Bradley Y and McKinney J M 2016 *Handbook of Radioembolization* (Boca Raton, FL: CRC Press)
- Sangro B *et al* 2008 Liver disease induced by radioembolization of liver tumours *Cancer* **112** 1539–46
- Seong J, Park H C, Han K H and Chon C Y 2003 Clinical results and prognostic factors in radiotherapy for unresectable hepatocellular carcinoma: a retrospective study of 158 patients *Int. J. Radiat. Oncol. Biol. Phys.* **55** 329–36
- Spreafico C, Maccauro M, Mazzaferro V and Chiesa C 2014 The dosimetric importance of the number of ^{90}Y microspheres in liver transarterial radioembolization (TARE) *Eur. J. Nucl. Med. Mol. Imaging* **41** 634–8
- Strigari L *et al* 2010 Efficacy and toxicity related to treatment of hepatocellular carcinoma with ^{90}Y SIR spheres: radiobiological considerations *J. Nucl. Med.* **51** 1377–85
- Tandon P and Garcia-Tsao G 2009 Prognostic indicators in hepatocellular carcinoma: a systematic review of 72 studies *Liver Int.* **29** 502–10
- Van Elmbt L, Vandenberghe S, Walrand S, Pauwels S and Jamar F 2011 Comparison of yttrium-90 quantitative imaging by TOF and non-TOF PET in a phantom of liver selective internal radiotherapy *Phys. Med. Biol.* **56** 6759

- Walrand S, Hesse M, Chiesa C, Lhommel R and Jamar F 2014a The low hepatic toxicity per Gray of ^{90}Y glass microspheres is linked to their transport in the arterial tree favoring a nonuniform trapping as observed in posttherapy PET imaging *J. Nucl. Med.* **55** 135–40
- Walrand S, Hesse M, Jamar F and Lhommel R 2014b A hepatic dose-toxicity model opening the way toward individualized radioembolization planning *J. Nucl. Med.* **55** 1317–22
- Wigg A J, Palumbo K and Wigg D R 2010 Radiotherapy for hepatocellular carcinoma: systematic review of radiobiology and modeling projections indicate reconsideration of its use *J. Gastroenterol. Hepatol.* **25** 664–71
- Willowson K P, Tapner M and Bailey D L 2015 A multicentre comparison of quantitative ^{90}Y PET/CT for dosimetric purposes after radioembolization with resin microspheres *Eur. J. Nucl. Med. Mol. Imaging* **42** 1202–22